International Journal of Heat and Mass Transfer 97 (2016) 101–109

Contents lists available at ScienceDirect

International Journal of Heat and Mass Transfer

journal homepage: www.elsevier.com/locate/ijhmt

# Vapour cooling of poorly conducting hot substrates increases the dynamic Leidenfrost temperature

Michiel A.J. van Limbeek [a,*,1], Minori Shirota [a,1], Pascal Sleutel [a], Chao Sun [a], Andrea Prosperetti [a,b], Detlef Lohse [a]

[a] Physics of Fluids, University of Twente, P. O. Box 217, 7500 AE Enschede, The Netherlands
[b] Department of Mechanical Engineering, Johns Hopkins University, Baltimore, MD 21218, USA

ARTICLE INFO

*Article history:*
Received 25 June 2015
Received in revised form 29 January 2016
Accepted 30 January 2016
Available online 17 February 2016

*Keywords:*
Spray cooling
Drop impact
High-speed TIR imaging
Non-isothermal transient heat-transfer

ABSTRACT

A drop impacting a smooth solid surface heated above the saturation temperature can either touch it (contact boiling) or not (film boiling), depending on the surface temperature. The heat transfer is greatly reduced in the latter case by the insulating vapour layer under the drop. In contrast to previous studies, here we use a relatively poor thermally conducting glass surface. Using a total internal reflection method, we visualise the wetting dynamics of the drop on the surface. We discover a new touch-down process, in which liquid–solid contact occurs a few hundred microseconds after the initial impact. This phenomenon is due to the cooling of the solid surface by the generation of vapour. We propose a model to account for this cooling effect, and validate it experimentally with our observations. The model leads to the determination of a thermal time scale (about 0.3 ms for glass) for the cooling of the solid. We conclude that when the impact time scale of the drop on the substrate (drop diameter/impact velocity) is of the order of the thermal time scale or larger, the cooling effect cannot be neglected and the drop will make contact in this manner. If the impact time scale however is much smaller than the thermal time scale, the surface remains essentially isothermal and the impact dynamics is not affected.


## 1. Introduction

In spray cooling applications and others, it is necessary to maintain contact between the droplets and the heated surface. As has been known for centuries [1,2], contact is abruptly lost once the surface of the hot solid exceeds a rather well defined value, called the Leidenfrost temperature $T_L$. This temperature depends on the thermo-physical properties of the liquid and the solid [3,4], the micro-structure of the surface [5,6] and the impact velocity $U$ [7]. In the static Leidenfrost case ($U = 0$), in which no impact dynamics are present, the lifetime of the drop is much longer than a thermal time scale $\tau_{th} = k_s \rho_s C_{p,s} h^{-2}$ [3,8,9]. Here, $\rho_s$ is the solid density, $k_s$ the thermal conductivity [W/(km)], $C_{p,s}$ the specific heat and $h$ the heat transfer coefficient from the solid to the drop. In general, the local cooling of the solid produced by the drop causes the Leidenfrost temperature $T_L$ to depend on the solid's thermal properties [3,8]. However, if the drop lifetime is shorter than $\tau_{th}$, the solid remains essentially isothermal and $T_L$ reaches a lower limiting value.

When the impacting drop has an initial downward velocity $U \neq 0$, the phenomenon is referred to as dynamic Leidenfrost effect. Due to its widespread applications, this dynamic case has drawn much interest [6,10–16]. By the dynamic pressure of the impact, the drop partly overcomes the cushioning of the vapour layer and only touches down at plate temperatures *higher* than the static $T_L$. The *dynamic* Leidenfrost temperature is found to depend on the drop size, impact velocity, liquid properties, surface roughness [11,13] and solid vibrations [12]. Some studies investigate scaling laws for the maximum radius of the deforming drop [11,13,17] or models for the time evolution of the impact dynamics [14,18,19].

The focus of this paper is the study of impacts on the smooth surface of glass, which has a relatively poor thermal conductivity and diffusivity, as little is known about how these features affect $T_L$. We experimentally examine the liquid–solid touch-down mechanism and how it is affected by the limited heat transfer supplied by the glass. The impacting liquid drop consists of ethanol and has an initial size $D_0$ and velocity $U$. We measure the thermal time scale $\tau_{th}$ and compare it with the impact time scale $\tau_{imp} = D_0/U$. At times larger than $\tau_{imp}$ all downward momentum is transferred into the radial direction and the drop is no longer

* Corresponding author.
[1] Both authors contributed equally on this publication.

http://dx.doi.org/10.1016/j.ijheatmasstransfer.2016.01.080
0017-9310/

forced into contact with the substrate. Our data shows that when $\tau_{th}$ is larger than $\tau_{imp}$, the substrate remains essentially isothermal. In the opposite case, the surface is appreciably cooled down by the (partial) evaporation of the drop and the cooling caused by the drop cannot be neglected. By using microdroplets instead of millimetre sized drops, we recover an isothermal impact, as $\tau_{imp} = D_0/U$ is then decreased by the decrease of the drop size.

**Table 1**
Relevant properties of ethanol and glass, and for comparison sapphire.

| Property | Units | Ethanol | Glass | Sapphire |
|---|---|---|---|---|
| Density $\rho$ | [kg/m$^3$] | 789 | 2520 | 3970 |
| Latent heat $L$ | [kJ/kg] | 837 | | |
| Specific heat $C_p$ | [kJ/kg K] | 2.4 | 816 | 776 |
| Surface tension $\sigma$ | [mN/m] | 23 | | |
| Thermal conductivity $k$ | [W/K m] | | 1 | 32 |
| Thermal diffusivity $\alpha$ | [m$^2$/s] | | $4 \times 10^{-7}$ | $1 \times 10^{-5}$ |
| $k\rho C_p$ | [J$^2$/K$^2$ s m$^4$] | | $2 \times 10^6$ | $1 \times 10^8$ |

## 2. Experimental setup and procedure

As sketched in Fig. 1, the experimental setup consists of a drop generator, a smooth and dry glass surface on which the drops impact, and two cameras to study the phenomenon.

Drops with a diameter between 2.1 and 2.6 mm are released from a needle from a variable height. The resulting impact velocity ranges between 0.4 m/s and 3.9 m/s, with corresponding Weber numbers $We = \rho_l U^2 D_0/\sigma_l$ between 16 and 1480; here $\rho_l$ and $\sigma_l$ are the liquid density and surface tension coefficient. We also study the impact of 300 μm-diameter microdroplets, which are generated as a continuous stream by an inkjet nozzle, with an impact velocity of 8.9 m/s. The stream is blocked by mechanical shutters, which can open briefly to allow a few drops to reach the surface. This arrangement also scatters the drops in space, so that they do not interact with each other during impact. In all experiments we measured both the diameter and impact velocity of each drop with a high speed camera (Photron Fastcam SA1.1) at 10 000 fps.

The ethanol drops impact a smooth glass microscope slide, the properties of which are listed in Table 1. In order to ensure constant temperature on the opposite side of the glass slide, we place a sapphire disc, which has a much higher thermal conductivity than glass, between the slide and the heater. The thermal penetration depth in the glass during the entire impact process can be estimated to be $\sqrt{\alpha_s \tau_{imp}} \approx 10$ μm, well below the 1 mm thickness of the slide. Before the impact, the slide surface is set at a temperature $T_{sur,0}$ from 80 °C to 590 °C by an electric heater; $T_{sur,0}$ was measured by a surface probe before each experiment. In view of the importance of the surface roughness for the Leidenfrost temperature (and the splashing threshold [20]), we measured by atomic force microscopy the RMS roughness of the glass slide, finding it smaller than 10 nm.

Next to the aforementioned side-view camera, we use two different imaging techniques to view the phenomena occurring during impact from below. In both techniques, the bottom view cameras (Photron SAX-2) were synchronised with the side view camera. The transparency of the setup enables us to use back light imaging through the substrate to obtain the bottom view (Fig. 1b). To measure the wetted area we use total internal reflection imaging (TIR), which was used previously in literature in both impact [20,21] and boiling studies [16,22]. Here, the light is coupled into the glass slide by a dove prism and, when the surface is dry, reflects from the top surface, so that all incident light enters the camera. However, if the surface is wetted by the drop, the refractive index changes from 1 (air) to 1.4 (ethanol) and the light can exit the slide through the drop, resulting in a dark spot on the camera. Just before the drop contacts the slide, it traverses the thickness of the evanescent wave, resulting in loss of intensity on the camera. As a consequence of the Fresnel equations, the intensity decreases exponentially with the distance from the slide surface, $I(y)/I(\infty) = 1 - \exp(-\beta y)$, where $\beta = 4\pi/(\lambda n)\sqrt{\sin^2\theta - n^2}$ [23]. In our case, $\beta = 80$ nm$^{-1}$ depending on wavelength $\lambda$, refractive index ratio $n = n_t/n_i$ (with $t$ and $i$ indicate transmitted and incident) and the incident angle $\theta$ of the laser beam with the normal of the surface. This circumstance permits us to map the local height of the drop surface over the slide from the light intensity measured by each pixel within 12.5% uncertainty (see Appendix B). We correct for light reflections from the droplet interface, according to Court and von Willisen [24]. By this TIR technique we can clearly distinguish whether or not portions of the drop under-surface are in direct contact with the slide. Using a long-distance microscope (Navitar 12× Telecentric variable zoom system) we obtained a field of view of 15 mm and 1 mm for the study of millimetric and microdrops respectively. The side view and bottom view are illuminated by a white light source, while for the TIR recordings a continuous

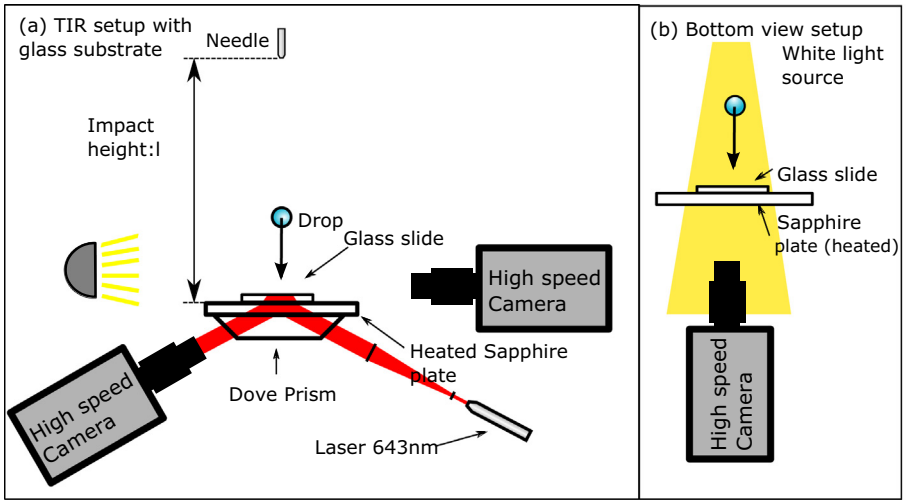


**Fig. 1.** Schematic of the experimental setups used: the total internal refraction (TIR) setup (a) and the bottom view setup (b).

red diode laser ($\lambda = 643$ nm) is used. The glass slide is optically coupled to the prism and sapphire disc by silicon oil to allow the laser light to propagate through all materials. The frame rate for the TIR imaging was 40 000 fps and we used a shutter speed of 300 ns to prevent motion blurring. In the microdroplet case, the TIR frame rate was increased to 100 000 fps for higher temporal resolution.

## 3. Results and discussion

### 3.1. Observations

Fig. 2 shows four examples of 2.6 mm-diameter drops impacting the glass slide at various temperatures with a velocity of $U = 1.3$ m/s ($We = 1293$). For each example, the sequence on the

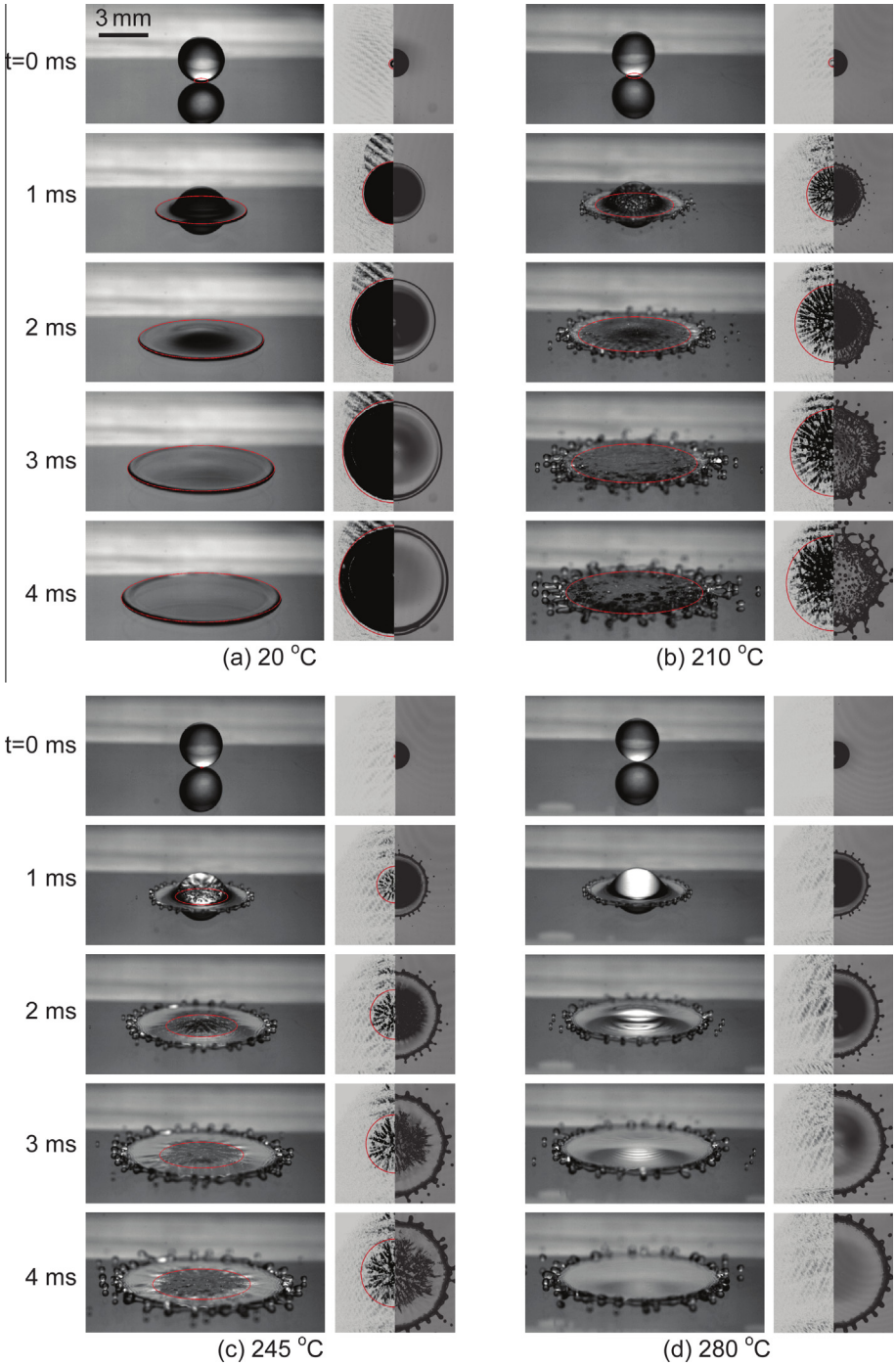


**Fig. 2.** Sequences of ethanol drops impacting on a glass substrate with velocity of 1.3 m/s. The substrate is at an initial temperature of $T_{sur,0} = 20$ (a), 210 (b), 245 (c) and 280 °C (d). In each sequence, the left images in each pair show the side-view, while the right ones are a composite of the bottom view (right part) and the total internal reflection TIR (left part) recordings. The red circles in the side-view represent the measured wetted area from the TIR recordings. Sequence (a) shows a typical cold case, where all three recordings reveal the same wetted area. Impacts in the transition regime are shown in sequences (b) and (c), where the contact line spreading is suppressed (TIR), while a lamella spreads and fragments as visible in the bottom view. Sequence (d) shows an impact in the Leidenfrost regime, with no touch-down, which cannot be deduced from the bottom view but is revealed by the TIR. Some 'shadows' in the TIR images are artefacts of the optical system. The movies can be found online [25]. (For interpretation of the references to colour in this figure caption, the reader is referred to the web version of this article.)

left shows the side view of the impact. The sequence on the right is a composite of the TIR recording (left half), which shows the wetted area, and the bottom view (right half). These images are recorded in different experiments. However, we are confident that both can be considered as showing essentially the same event due to the repeatability of the experiment and to the fact that both recordings are synchronised with the side view.

For impacts from room temperature (Fig. 2a) up to 186 °C we observe the spreading of the drops on the solid surface to proceed at velocities similar to those reported in previous studies of the impact on cold surfaces [26–28]. The radius from the TIR data corresponds to that of the moving contact line, represented by a red circle, in both the bottom and side views. Heating the substrate further changes this correspondence: at 210 °C we see that the growth of the wetted area is suppressed: the drop liquid is now partially levitating above the solid surface, forming a lamella which hovers over its own vapour (Fig. 2b). As the drop is now partly levitating and partly touching the solid, it is in a transitional state between contact and Leidenfrost boiling. With increasing temperature, the wetted area shrinks further (Fig. 2c) until at 280 °C the surface is never wetted by the drop, which is thus in the Leidenfrost state (Fig. 2d). This sequence of behaviours with increasing temperature is sketched in Fig. 3a.

In the transition boiling regime, the TIR recordings show a fingering pattern (Fig. 2b and c), as reported for earlier experiments on glass [16]. However, preliminary results (not shown here) for impacts on a sapphire plate with a comparable smoothness do not exhibit this fingering pattern [14]. As sapphire is a better thermal conductor than glass, these observations suggest that the thermal properties of the substrate play a role in the appearance of this pattern.

As exemplified in Fig. 2, for each surface temperature $T_{sur,0}$, the bottom views (rightmost images) provide information on the spreading front of the drop and on the wetted area. We define the radius $R_s(t)$ of the spreading front as the radius of the dark circle marking the edge of the drop in the bottom view images. The radius $R_w(t)$ of the wetted area is defined as the radius of the smallest circle encompassing the wetted area, as shown by the red circle in the figure. The data obtained in this way are shown in Fig. 3 for various surface temperatures up to the incipience of the Leidenfrost state. We find that $R_s(t)$ (Fig. 3b) increases only slightly with increasing $T_{sur,0}$. At the lower temperatures, $R_w(t)$ (Fig. 3c) keeps pace with $R_s(t)$. However, from the start of the transition regime at 203 °C, this correspondence between the two quantities is lost and $R_w(t)$ grows much less than $R_s(t)$. At the end of the transition regime, $R_w$ settles at about 0.75 $D_0$. Above 266 °C, no wetting is found and the drops are in the Leidenfrost state. It is also noteworthy that a non-monotonic increase of $R_s$ with $T_{sur,0}$ is found in Fig. 3b for $t/\tau_{imp} > 1$. This is caused by the lamella breakup which is strongest at the beginning of the transition boiling as shown in Fig. 2.

We performed experiments for different impact velocities as well. The observed boiling behaviours are plotted in the phase space $(U, T_{sur,0})$ in Fig. 4. Three main regions can be identified: for low substrate temperatures we find stable contact boiling, represented by blue circles. Here, the growth of the wetted area keeps pace with the spreading as for impact on unheated surfaces. In orange we indicate the aforementioned transition region where a lamella is ejected. Here, the wetting velocity of the contact line lags behind the expansion rate of the lamella. This regime is characterised by two different behaviours, indicated by △ and ◊, to be discussed later. For high temperatures we find no wetted area and the impacts are in the Leidenfrost state, shown as red squares.

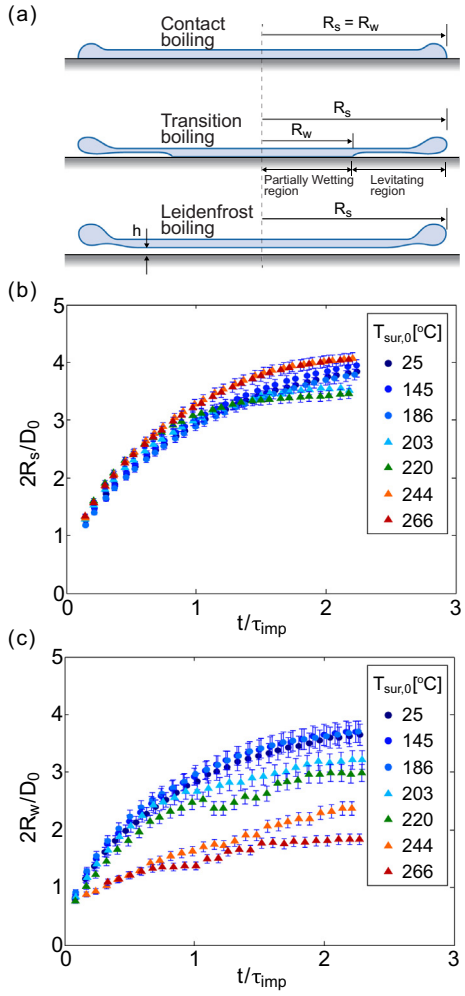


**Fig. 3.** (a) Schematic of the three different spreading states: contact, transition and Leidenfrost boiling, indicating the difference between the radius of the wetted area $R_w$ and spreading front $R_s$ (within 5 and 10% uncertainty, see Appendix A). Observed time evolution of $R_s$ (b) and $R_w$ (c) of ethanol drops impacting at $U = 1.3$ m/s for increasing surface temperatures. Data for cold and contact boiling is indicated by °. For contact boiling $R_w = R_s$, while the lamella speed increases in the transition regime △; the wetting speed instead decreases, as compared to °. Later ($t = 2$ ms), the lamella spreading stalls due to fragmentation (see Fig. 2b). The absence of wetting above 266 °C shows the drops to be in the Leidenfrost state. Details on errorbars can be found in Appendix A.

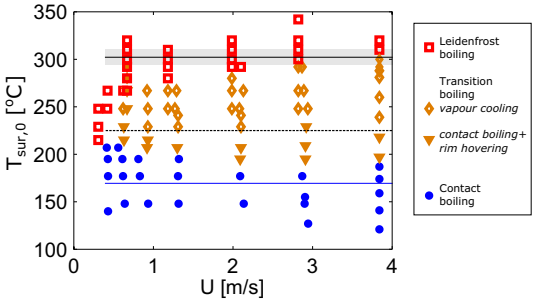


**Fig. 4.** Phase space with an indication of the different boiling behaviours. The dashed line is a guide to the eye, indicating the boundary between *contact boiling + rim hovering* and *vapour cooling*. The solid black line denotes the transition to the Leidenfrost state, according to Eq. (2); the shaded area indicates the estimated error. The Leidenfrost transition for isothermal impacts on sapphire is shown for comparison by the blue line at $T_{sur,0} = 170$ °C (data from Staat et al. [15]). (For interpretation of the references to colour in this figure caption, the reader is referred to the web version of this article.)

### 3.2. Subcooling effect causes touch-down

The points denoted by △ in the phase space of Fig. 4 indicate drops that, even though partially levitated, immediately exhibit stable boiling on the wetted area; this regime is indicated as *contact boiling + rim hovering* in the legend of the figure. This behaviour is strikingly different from that of drops that levitate at the very beginning of the impact, but then touch down at a later time. This regime, to which we refer as *vapour cooling*, is marked by ◊ in Fig. 4. A detailed example of the drop behaviour in this case is shown in Fig. 5a; the drop diameter is 2.3 mm, the impact velocity $U = 3.84$ m/s and the glass slide temperature $T_{sur,0}$ is 292 °C. For each frame in this figure, the upper half shows the TIR image, while the lower half is the reconstructed height profile of the underside of the drop in tens of nm resolution. Here the drop first remains levitated (i–iv), but in frames (v) and (vi) it starts to randomly touch the surface, exhibiting what may be called unstable boiling. This behaviour is different from what we earlier referred to as stable boiling in which the liquid–solid contact does not fluctuate appreciably. Later, the drop wets the surface and a stable fingering pattern is observed, as discussed before. It is also interesting to note that no drop is visible in frame (ii), although it reappears in frame (iii). This behaviour implies that the pressure under the drop is initially so large as to briefly push it back. We have encountered this phenomenon only in the upper range of the temperatures investigated.

This delayed touch-down mechanism is due to the cooling that the vapour generation induces in the solid. Due to the small thermal conductivity of glass, $T_{sur}(t)$ drops significantly during the early stages of the impact to such an extent that the drop levitation cannot be maintained. Such effects of the solid thermal properties are frequently encountered in heat transfer phenomena. Examples are the influence of the thermal conductivity of a hot metal being wetted by the advancing front of a cold liquid [29,30], the similar effect of the substrate influencing the waiting time between two successive bubbles in boiling [31] and the reduction of the Nusselt number in turbulent thermal convection [32].

The situation that is established during the drop impact is characterised by the very short distance (less than 1 μm) that separates the liquid surface from the solid and a much longer scale parallel to

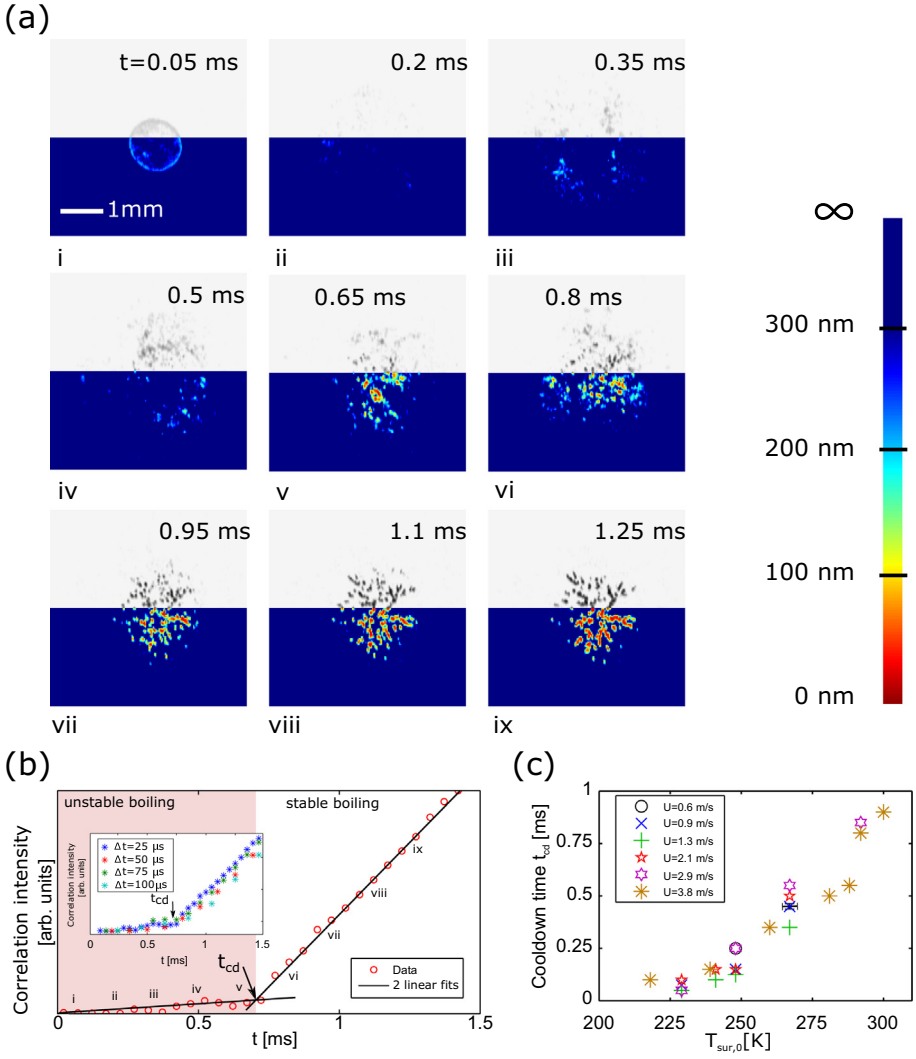


**Fig. 5.** (a) TIR data of an ethanol drop, with a diameter of 2.3 mm, impacting at $U = 3.8$ m/s a heated glass surface of $T_{sur,0} = 292$ °C. The upper half of each frame shows the measured light intensity. As explained in the text, from these data we deduce the local height of the drop surface above the solid, i.e., the local thickness of the vapour layer, which is shown in the lower half (with 9% uncertainty, see Appendix B). The sequence shows the change from levitation (i–iv) to unstable contact (v,vi) to eventually stable boiling (vii–ix). The absence of the signal in (ii) results from a brief upward motion of the drop surface, only observed for high surface temperatures (b): Time series of the correlation coefficient for the data shown in (a) with matching roman numerals. The inset shows the effect of correlating pairs of non-consecutive images separated by 1–3 frames. (c): Measured cool-down times (defined in the text) for various impact velocities as a function of initial substrate temperature. For clarity, only one set of error bars is shown.

the solid surface. This large scale separation justifies the use of a one-dimensional conduction model in the solid. We assume the drop surface to remain at the saturation temperature $T_b$ and model the heat flux out of the solid as $h(T_{sur}(t) - T_b)$, where $h$ is a heat transfer coefficient. We may expect $h$ to be enhanced beyond the pure conduction value ($k_v/\delta_v$, with $k_v$ the thermal conductivity of the vapour and $\delta_v$ the thickness of the vapour layer) by the vapour flow between the drop and the surface, although the order of magnitude should not be altered. This expectation is based on the well known relation of the Nusselt number for fully developed laminar flow in ducts [33]. The solution of the conduction problem thus posed is well known [3,34–36]. The temperature of the solid surface $T_{sur}(t)$ is found to be given by:

$$\frac{T_{sur}(t) - T_b}{T_{sur,0} - T_b} = \exp\left(\frac{t}{\tau_{th}}\right)\mathrm{erfc}\left(\sqrt{\frac{t}{\tau_{th}}}\right), \quad (1)$$

in which the characteristic thermal time scale is given by $\tau_{th} = k_s\rho_s C_{p,s} h^{-2}$.

In order to determine $\tau_{th}$, as the heat transfer coefficient $h$ is unknown for our system, for each experiment we measure the cool-down time $t_{cd}$, i.e., the time before stable contact boiling is observed. Then we apply Eq. (1) to fit our data and obtain $\tau_{th}$ from which we calculate $h$. The cool-down time $t_{cd}$ is obtained by studying the temporal correlation coefficient between image pairs. This coefficient is a measure of the degree of similarity between two successive frames. For $t < t_{cd}$ the drop is either still levitating or randomly touching the substrate. The wetted area is then rapidly varying and the resulting correlation between successive images is poor. When the surface is cooled down by the evaporation, on the other hand, the wetted patches become more stable, resulting in a high correlation coefficient. We used sequences such as that of Fig. 5a to create a time series of correlation coefficients, an example of which is shown in Fig. 5b. Here, the sudden increase in correlation is readily identifiable as occurring for $t \approx 0.7$ ms, where two straight lines fitted to the correlation data intersect. Skipping frames (inset) reveals that the technique is fairly insensitive to the frame rate (provided, of course, it is not too short). We apply this technique to measure $t_{cd}$ for various impact velocities and initial plate temperatures $T_{sur,0}$. The results are presented in Fig. 5c and show that, for higher temperatures, it takes more time for the surface to cool down to the temperature level required for stable boiling. Furthermore, the data for different impact velocities exhibit a near-collapse. This is in agreement with the dashed line in Fig. 4 being independent of velocity as well. Both observations indicate that the cooldown time is at most weakly dependent on the impact velocity. However we do observe for high initial surface temperatures only stable boiling for high impact velocities. This is due to the higher dynamic pressure, forcing the drop more strongly towards the surface [28,37].

Once $t_{cd}$ has been determined, we can proceed to use the information to estimate the thermal time scale $\tau_{th}$ appearing in Eq. (1). Since for $t = t_{cd}$ the surface temperature becomes too low to support the drop we deduce that, at this instant, the surface temperature equals the static Leidenfrost temperature for isothermal surfaces, i.e., $T_{sur}(t = t_{cd}) = 160\,^\circ$C [3]. We plot in Fig. 6 for each experiment $(160\,^\circ\mathrm{C} - T_b)/(T_{sur,0} - T_b)$ against $t_{cd}$ . The black lines correspond to various solutions of Eq. (1) and the best fit of the data is the blue line with $\tau_{th} = 0.3$ ms. The fit is not very sensitive in this range either to the precise value of $t_{cd}$ or to the value assumed for the static isothermal Leidenfrost temperature. Although the fit is reasonably close to the data, there seems to be some difference between large and small values of $t_{cd}$, which corresponds to a slight increase of the thermal time scale with $t_{cd}$ and, therefore, with $T_{sur,0}$. This results implies that the average heat transfer coefficient decreases somewhat with increasing surface

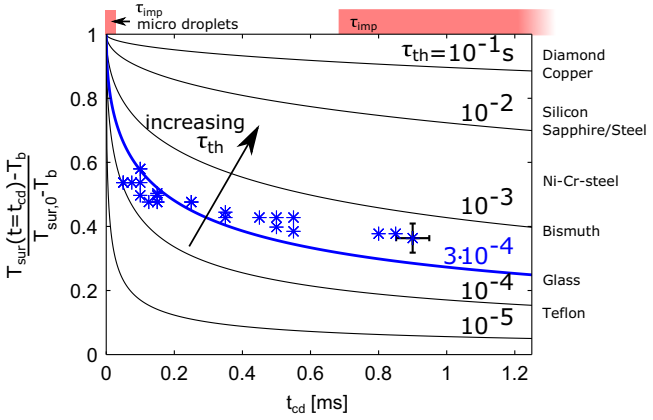


**Fig. 6.** As argued in the text, for $t = t_{cd}$, the surface temperature $T_{sur}(t_{cd})$ should equal 160 °C. The asterisks show the value $(T_{sur}(t_{cd}) - T_b)/(T_{sur,0} - T_b)$ for various values of $T_{sur,0}$, in correspondence of the $t_{cd}$ measured in each experiment, as presented in Fig. 5c. For clarity, only one set of error bars is shown. The best fit of the data by Eq. (1) is presented by the thick blue line; the remaining black lines present other solution corresponding with different thermal time scales. These solutions match various materials listed on the right, assuming that for impacts on smooth materials the heat transfer coefficient through the vapour layer has the constant value measured in the present study (here $8 \times 10^4$ W/(m$^2$)). The red areas at the top of the figure indicate the impact time scales examined here for micro- and millimetric drops. (For interpretation of the references to colour in this figure caption, the reader is referred to the web version of this article.)

temperature. Possible causes can be a larger initial vapour layer thickness as would be implied by the behaviour described before in connection with frame (ii) of Fig. 5a and increased convection cooling by the vapour.

It is interesting to compare the thermal time scale $\tau_{th}$ with the time $\tau_{imp} = D_0/U$ characteristic of the impact, by which all the downward momentum is converted into the radial direction and the dynamic pressure vanishes [38]. This is also the longest time the residual momentum can maintain the drop against the hot surface. Thus, if $\tau_{th}$ is equal or smaller than $\tau_{imp}$, the surface will cool down significantly. This is the case for all the impacts of millimetric drops studied here, for instance: in Fig. 5 $\tau_{imp} = 0.6$ ms which is approximately $\tau_{th}$.

From the thermal time scale $\tau_{th}$ we can deduce an estimate for the heat transfer coefficient $h = \sqrt{(k_s\rho_s C_{p,s}/\tau_{th})}$, which is therefore found to be $8 \times 10^4$ W/(m$^2$K). For pure conduction through the vapour layer, this result corresponds to a thickness $\delta_v \approx 100$ nm. This estimate is in agreement with our measurements of the minimum vapour thickness (for example Fig. 5) obtained from the evanescence wave attenuation length. Furthermore, assuming that this thickness is typical for impacts on smooth surfaces, one can now predict whether or not an impact can be considered as isothermal: the impact conditions yield $\tau_{imp}$ and one estimates $\tau_{th} = (100\ \mathrm{nm}/k_v)^2 k_s\rho_s C_{p,s}$ from the surface properties. The surface cooling for various materials based on their estimated $\tau_{th}$ is shown in Fig. 6.

Focussing in more detail on the phase space of Fig. 4, we now aim to predict the boundary between the transition region (orange) and the Leidenfrost region (red). For all impact velocities we select the lowest surface temperature resulting in the Leidenfrost state and measure the time that the drop is within 100 nm distance of the substrate, see Table 2. The average time observed is 0.51 ms without any significant velocity dependence, in accordance with our previous observations (Fig. 5c). This 'residence time' is typically shorter than $\tau_{imp}$. Using these observations, we can calculate $T_{sur,0}$ by solving Eq. (1) with $T_{sur}(t = 0.51\ \mathrm{ms}) = 160\,^\circ$C, the static isothermal $T_L$ for ethanol:

**Table 2**
Observed residence time of the drop within 100 nm from the solid surface for impact on a glass slide. The last column is the estimated Leidenfrost temperature obtained similarly to (2), using for the residence time the value listed in column four in place of 0.51 ms.

| $U$ [m/s] | $We = \rho_l U^2 D_0/(2\sigma_l)$ | Lowest $T_L$ [°C] | Residence time [ms] | $T_L$ by Eq. (2) [°C] |
|---|---|---|---|---|
| 0.4 | 8 | 267 | 0.4 | 285 ± 10 |
| 0.6 | 27 | 280 | 0.45 | 294 ± 10 |
| 1.3 | 111 | 280 | 0.6 | 318 ± 10 |
| 2.1 | 279 | 290 | 0.55 | 310 ± 10 |
| 2.9 | 538 | 300 | 0.5 | 303 ± 10 |
| 3.8 | 740 | 310 | 0.6 | 318 ± 10 |

$$T_{sur,0} = \frac{160\,^\circ\mathrm{C} - 80\,^\circ\mathrm{C}}{\exp(0.51/0.3)\,\mathrm{erfc}\left(\sqrt{0.51/0.3}\right)} + 80\,^\circ\mathrm{C} = 304\,^\circ\mathrm{C}. \quad (2)$$

The obtained prediction is plotted in Fig. 4 by a black solid line; the shaded area indicates the estimated error. We see that including this correction for the non-isothermal behaviour of the solid yields a good prediction for the dynamic Leidenfrost temperature.

### 3.3. Micro droplets show isothermal behaviour

The previous analysis assumed the elevated Leidenfrost temperature found for impacts on a glass surface to originate from the thermal properties of the substrate. In order to strengthen this conclusion, we also studied the case in which $\tau_{imp} \ll \tau_{th}$ by considerably shortening the impact time scale $\tau_{imp}$. This objective is achieved by using microdroplets, as the smaller diameter $D_0 = 300$ µm lowers $\tau_{imp} = D_0/U$ to 30 µs, satisfying $\tau_{imp} \ll \tau_{th}$. In this case we expect even a glass substrate to behave as isothermal with no observable cool-down effect. A sequence showing the full impact and spreading phases of a microdrop impacting at $U = 8.9$ m/s a glass surface with $T_{sur,0} = 265\,^\circ$C (just below $T_L$) is shown in Fig. 7.

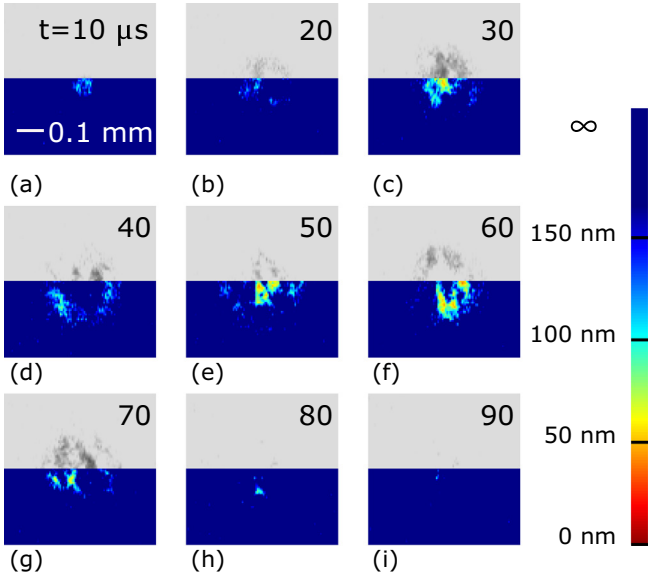


**Fig. 7.** Similarly to Fig. 5, each frame is a composite of the TIR-measured light intensity and the corresponding thickness (with 12.5% uncertainty, see Appendix B) of the vapour film for an 300 µm-diameter ethanol droplet impacting a glass substrate just below the Leidenfrost temperature $T_{sur,0} = 265\,^\circ$C. The impact velocity is 8.9 m/s ($We = 1874$). No stable boiling is observed as $\tau_{imp} \approx 30$ µs, which is much shorter than $\tau_{th}$.

Comparing the results with the millimetric drops shown in Fig. 5, we first observe a levitating droplet as well. From $t = 50$ µs on, the drop touches the surface randomly. However, in contrast with the millimetric case, no stable boiling is observed for the microdroplet impact. Varying the impact velocity between 2 and 8.9 m/s, we did not observe any cool-down effect. In this case, the touch-down mechanism then is purely governed by the impact dynamics, as expected from the estimate of the time scales. We conclude therefore that the same surface that exhibits cooling with large drops, behaves as isothermal when the time scale of the impact dynamics is shorter than the thermal time scale.

## 4. Conclusions

We studied the impact of ethanol drops on superheated smooth glass substrates. We used high speed total internal reflection imaging to study the dynamics of the wetted area of the surface. We observed a new touch-down mechanism for millimetric drops caused by the cooling of the solid surface. By comparing the time scale $\tau_{th}$ for the cooling of the glass surface with the impact time scale $\tau_{imp} = D_0/U$ we concluded that a millimetric drop causes a significant cooling the glass surface. While the drop remains levitated during the early stages of the impact, this cooling causes it to eventually touch the solid. By means of a one-dimensional conduction model, we developed an estimate of the dynamic Leidenfrost temperature for a poorly conducting solid. We calculated $\tau_{th}$ for glass to be 0.3 ms, which is well below $\tau_{imp}$ for the impact events studied here. For impact velocities in the range of 0.6–3.8 m/s, investigated in this study, the vapour thickness calculated from $\tau_{th}$ is approximately 100 nm, consistent with our measurements. Using this information, together with the substrate properties one can thus a priori estimate the thermal time scale.

The previous conclusions are consistent with the results of another set of experiments on the impact of micro-droplets for which $\tau_{imp}$ is much shorter than $\tau_{th}$. In this case, indeed, we do not observe any cooling effect and the surface remains essentially isothermal.

To summarise, therefore, for $\tau_{imp} \ll \tau_{th}$, the solid remains essentially isothermal and the touch-down of the drop is governed by the dynamic pressure of the impact. For $\tau_{imp} \geqslant \tau_{th}$, on the other hand, the substrate is cooled during the spreading of the drop, which eventually touches the solid surface.

## Acknowledgements

This work was partially supported by Fundamenteel Onderzoek der Materie, NanoNextNL and by an ERC Advanced Grant.

## Appendix A. Image processing

The three types of recordings we obtain in our experiments are processed in different ways, using Matlab programming. The side-view images are used for the measurements of the diameter and impact velocity by a simple edge detection technique. The classification of the boiling regimes are done manually by comparing all three image types by characteristics as explained in details in Section 3.1.

The image analysis of the TIR data consists mainly of two processes: firstly, the image transformation and secondly the detection of the wetted area, as shown in Fig. A.8(a–f). Even though a droplet wets the substrate in an axisymmetric manner, the TIR image gives an ellipsoid as shown in (a), due to the optical transformations in the setup. The original image is first binarized after background subtraction as shown in (b). From the binary image, the angle of rotation and aspect ratio are measured; for this

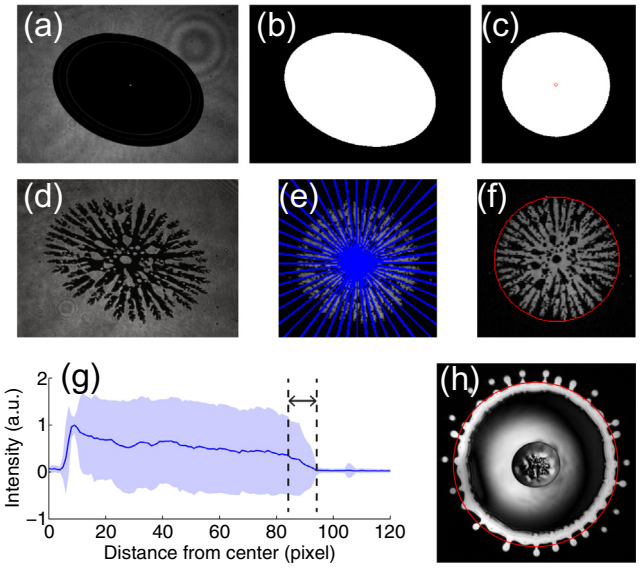


**Fig. A.8.** Typical examples of (a–c) images used for calibration of TIR image transform, (d–f) TIR images in transition boiling regime showing the transformation with the rate given in (a–c), (g) average intensity (solid line) together with standard deviation (shaded area) along the lines radially spread outward from the centre of wetted area (blue lines in (e)), and (h) an image of bottom view with backlighting after the background subtraction. The red circles in (f) and (h) show the detected wetting and spreading front, respectively. The uncertainty caused by the non-uniform growth rate of the fingers is shown by the arrow in (g). (For interpretation of the references to colour in this figure caption, the reader is referred to the web version of this article.)

measurement, the frame corresponding to $t/t_{imp} = 0.25$ of room temperature experiment was typically used. Using the linear transformation, the circular droplet, (c), is reconstructed.

The linear transformation obtained from the room temperature experiment was also used in the analysis of different temperature cases. A typical example of impact on a heated surface is shown in Fig. A.8(d–f), where the initially ellipsoidal fingering pattern in (d) is well transformed back to the circular one in (f). Note here that the envelope circle shown as the red line in (f) was determined from the average-intensity profile, such as shown in (g), as the point of abrupt decrease in mean value (solid line) and standard deviation (shaded area); the intensity profile was calculated from intensities along 50–100 lines spreading radially outward from the droplet centre, see (e).

The radius of spreading front $R_s$ was also determined from the bottom-view image as in the same manner for TIR analysis except for the linear transformation. We set the thresholding condition in such a way that the foot of the fingers at the rim of the droplet was detected as shown by the red circle in Fig. A.8(h).

The main cause of the uncertainty of the radius of the spreading front $R_s$ arises from the non-uniform growth rate of the fingers pinched off from the peripheral rim; such non-uniform behaviour result in an uncertainty for defining the spreading front from the image intensity profile, a typical example of which is shown by the arrow in Fig. A.8(g). Similarly, for the radius of the wetting area $R_w$, the non-uniform wetting rate of the fingering pattern causes the largest uncertainty. In summary, the uncertainty is, at most, 5% for $R_s$ and 10% for $R_w$.

## Appendix B. Error estimate of the measured height from TIR measurement

Starting from the equation for the height $h$ and the normalised intensity [24]: $I' = \frac{I}{I_\infty} = EE^*$, with $E$ being the electric field and $E^*$ its complex conjugate.

$$h = -\beta \ln\left(\frac{r_{12} - E}{r_{32} - r r_{12} r_{32}}\right), \tag{B.1}$$

$$\text{where } \beta = \frac{\lambda}{4\pi} \frac{n}{\sqrt{\sin(\theta_i)^2 - n^2}} \tag{B.2}$$

Here $\lambda$ is 643 nm, the wavelength of the light source, $n = 1/1.51$ the ratio of refractive indices of the air and glass and $\theta_i$ is the angle between the laser light and the normal of the glass surface, resulting in $\beta = 81$ and 59 nm$^{-1}$, with $\theta_i = 52°$ and 61°, for the millimetric drops and micro droplet measurements respectively. The functions $r_{12}$ and $r_{32}$ are the reflectivity coefficients as given by the Fresnel equations for the solid–air and air–liquid interface for $p$-polarised light respectively. These functions depend on $n, \theta_i$ and $n_d$, the refractive index of the droplet liquid. We then calculate numerically the error which is presented in Fig. B.9.

Here the following uncertainties are used to estimate the total error: $\Delta\lambda = 0.5$ nm, $\Delta n_{ti} = 0.001$ where the refractive index was evaluated from room temperature to 400 °C [39], and $\Delta\theta_i = 0.5°$ from our analysis uncertainty. We estimate the error in the measured intensity to be 2% originating from fluctuations in the laser intensity. From this analysis, we can approximate the error $\Delta h$ to increases linearly with height. The average relative error $\Delta h/h$ is

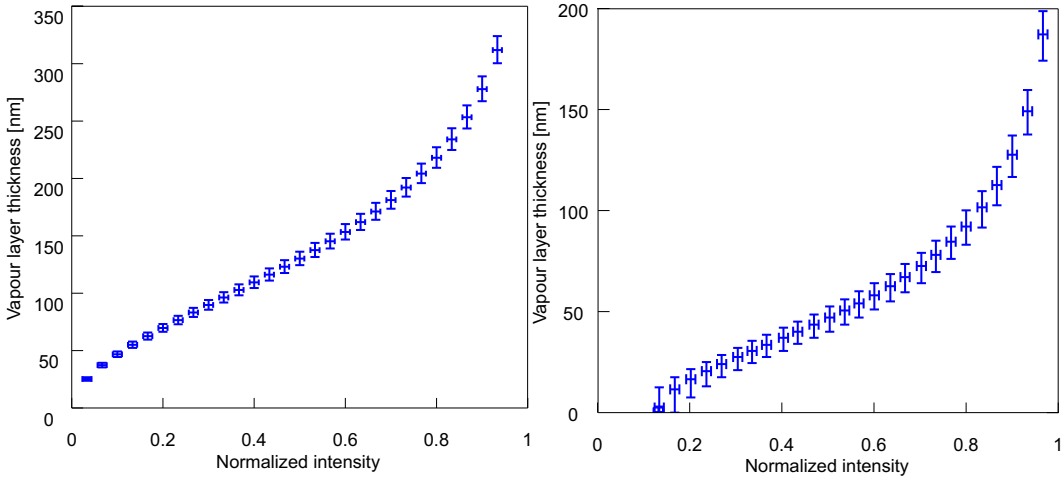


**Fig. B.9.** Error estimate for the millimetric (left) and micro droplet (right) measurements. The vertical errorbars the combined uncertainties in refractive indices, laser wavelength and angle of incidence of the laser.

9% for millimetric drops and 12.5% for the micro droplet measurements.

## Appendix C. Supplementary data

Supplementary data associated with this article can be found, in the online version, at http://dx.doi.org/10.1016/j.ijheatmasstransfer.2016.01.080.

## References


[1] J.G. Leidenfrost, De aquae communis nonnullis qualitatibus tractatus, Ovenius, Duisburg, 1756.
[2] D. Quéré, Leidenfrost dynamics, Annu. Rev. Fluid Mech. 45 (2013) 197–215.
[3] K. Baumeister, F. Simon, Leidenfrost temperature—its correlation for liquid metals, cryogens, hydrocarbons, and water, J. Heat Transfer 95 (1973) 166–173.
[4] J.D. Bernardin, I. Mudawar, The Leidenfrost point: experimental study and assessment of existing models, J. Heat Transfer 121 (1999) 894–903.
[5] H. Kim, B. Truong, J. Buongiorno, L.-W. Hu, On the effect of surface roughness height, wettability, and nanoporosity on Leidenfrost phenomena, Appl. Phys. Lett. 98 (2011) 083121.
[6] H.-M. Kwon, J.C. Bird, K.K. Varanasi, Increasing Leidenfrost point using micro–nano hierarchical surface structures, Appl. Phys. Lett. 103 (2013) 201601.
[7] T. Tran, H.J.J. Staat, A. Prosperetti, C. Sun, D. Lohse, Drop impact on superheated surfaces, Phys. Rev. Let. 108 (2012) 036101.
[8] L.H.J. Wachters, H. Bonne, H.J. van Nouhuis, The heat transfer from a hot horizontal plate to sessile water drops in the spherodial state, Chem. Eng. Sci. 21 (1966) 923–936.
[9] A.-L. Biance, C. Clanet, D. Quéré, Leidenfrost drops, Phys. Fluids 15 (2003) 1632–1637.
[10] H. Fujimoto, Y. Oku, T. Ogihara, H. Takuda, Hydrodynamics and boiling phenomena of water droplets impinging on hot solid, Int. J. Multiphase Flow 36 (2010) 620–642.
[11] H. Nair, H.J.J. Staat, T. Tran, A. van Houselt, A. Prosperetti, D. Lohse, C. Sun, The Leidenfrost temperature increase for impacting droplets on carbon-nanofiber surfaces, Soft Matter 10 (2014) 2102–2109.
[12] B.T. Ng, Y.M. Hung, M.K. Tan, Suppression of the Leidenfrost effect via low frequency vibrations, Soft Matter 11 (2015) 775–784.
[13] T. Tran, H.J.J. Staat, A. Susarrey-Arce, T.C. Foertsch, A. van Houselt, H.J.G.E. Gardeniers, A. Prosperetti, D. Lohse, C. Sun, Droplet impact on superheated micro-structured surfaces, Soft Matter 9 (2013) 3272–3282.
[14] M. Shirota, M.A.J. van Limbeek, C. Sun, A. Prosperetti, D. Lohse, Dynamic Leidenfrost effect: relevant time and length scales, Phys. Rev. Let. 116 (2016) 064501.
[15] H.J.J. Staat et al., Phase diagram for droplet impact on superheated surfaces, J. Fluid Mech. 779 (2015) R3.
[16] M. Khavari, C. Sun, D. Lohse, T. Tran, Fingering patterns during droplet impact on heated surfaces, Soft Matter 11 (2015) 3298–3303.
[17] A.-L. Biance, F. Chevy, C. Clanet, G. Lagubeau, D. Quéré, On the elasticity of an inertial liquid shock, J. Fluid Mech. 554 (2006) 47–66.
[18] H. Lastakowski, F. Boyer, A.-L. Biance, C. Pirat, C. Ybert, Bridging local to global dynamics of drop impact onto solid substrates, J. Fluid Mech. 747 (2014) 103–118.
[19] E. Villermaux, B. Bossa, Drop fragmentation on impact, J. Fluid Mech. 668 (2011) 412–435.
[20] J.M. Kolinski, L. Mahadevan, S.M. Rubinstein, Drops can bounce from perfectly hydrophilic surfaces, Europhys. Lett. 108 (2014) 24001.
[21] J.M. Kolinski, S.M. Rubinstein, S. Mandre, M.P. Brenner, D.A. Weitz, L. Mahadevan, Skating on a film of air: drops impacting on a surface, Phys. Rev. Lett. 108 (2012) 074503.
[22] J. Kim, Spray cooling heat transfer: the state of the art, Int. J. Heat Fluid Flow 28 (2007) 753–767.
[23] E. Hecht, Optics, fourth ed., Addison Wesley Longman Inc, Boston, 1998.
[24] I.N. Court, F.K. von Willisen, Frustrated total internal reflection and application of its principle to laser cavity design, Appl. Opt. 3 (6) (1964) 719–726.
[25] M.A.J. van Limbeek, M. Shirota, P. Sleutel, C. Sun, A. Prosperetti, D. Lohse, Vapour cooling of poorly conducting hot substrates increases the dynamic Leidenfrost temperature, Int. J. Heat Mass Transfer 97 (2016) 101–109.
[26] S. Mandre, M. Mani, M.P. Brenner, Precursors to splashing of liquid droplets on a solid surface, Phys. Rev. Lett. 102 (2009) 134502.
[27] S. Mandre, M.P. Brenner, The mechanism of a splash on a dry solid surface, J. Fluid Mech. 690 (2012) 148–172.
[28] G. Riboux, J.M. Gordillo, Experiments of drops impacting a smooth solid surface: a model of the critical impact speed for drop splashing, Phys. Rev. Lett. 113 (2014) 024507.
[29] R.B. Duffey, D.T.C. Porthouse, The physics of rewetting in water reactor emergency core cooling, Nucl. Eng. Des. 25 (1973) 379–394.
[30] M.K. Agrawal, S.K. Sahu, Analysis of conduction-controlled rewetting of a hot surface by variational method, Heat Mass Transfer 49 (2013) 963–971.
[31] V.K. Dhir, Mechanistic prediction of nucleate boiling heat transfer–achievable or a hopeless task?, J Heat Transfer 128 (2006) 1–12.
[32] R. Verzicco, Effects of nonperfect thermal sources in turbulent thermal convection, Phys. Fluids 16 (2004) 1965–1979.
[33] A. Bejan, Heat Transfer, first ed., John Wiley @ Sons Inc, New York, 1993.
[34] S. Chandra, C. Avedisian, On the collision of a droplet with a solid surface, Proc. R. Soc. Lond. A: Math. Phys. Eng. Sci. 432 (1991) 13–41.
[35] H. Carslaw, J. Jaeger, Conduction of Heat in Solids, first ed., Clarendon Press, Oxford, 1959.
[36] Y. Qiao, S. Chandra, Boiling of droplets on a hot surface in low gravity, Int. J. Heat Mass Transfer 39 (1996) 1379–1393.
[37] J. Philippi, P.-Y. Lagrée, A. Antkowiak, Drop impact on a solid surface: short time self-similarity, 2015. <arXiv:1504.05847v1>.
[38] M. Mani, S. Mandre, M.P. Brenner, Events before droplet splashing on a solid surface, J. Fluid Mech. 647 (2010) 163–185.
[39] T. Toyoda, M. Yabe, The temperature dependence of the refractive indices of fused silica and crystal quartz, J. Phys. D 16 (1983) L97L100.